

UPHDR-GAN: Generative Adversarial Network for High Dynamic Range Imaging with Unpaired Data

Ru Li^a, Chuan Wang^b, Shuaicheng Liu^a, Jue Wang^b, Guanghui Liu^a, Bing Zeng^a

^a*School of Information and Communication Engineering, University of Electronic Science and Technology of China, Chengdu 611731, China*

^b*Megvii Technology, Chengdu 610000, China*

Abstract

The paper proposes a method to effectively fuse multi-exposure inputs and generates high-quality high dynamic range (HDR) images with unpaired datasets. Deep learning-based HDR image generation methods rely heavily on paired datasets. The ground truth provides information for the network getting HDR images without ghosting. Datasets without ground truth are hard to apply to train deep neural networks. Recently, Generative Adversarial Networks (GAN) have demonstrated their potentials of translating images from source domain X to target domain Y in the absence of paired examples. In this paper, we propose a GAN-based network for solving such problems while generating enjoyable HDR results, named UPHDR-GAN. The proposed method relaxes the constraint of paired dataset and learns the mapping from LDR domain to HDR domain. Although the pair data are missing, UPHDR-GAN can properly handle the ghosting artifacts caused by moving objects or misalignments with the help of modified GAN loss, improved discriminator network and useful initialization phase. The proposed method preserves the details of important regions and improves the total image perceptual quality. Qualitative and quantitative comparisons against other methods demonstrated the superiority of our method.

Keywords: Multi-exposure HDR imaging, generative adversarial network, unpaired data



Figure 1: LDR images with different exposures are shown in (a), and our result is shown in (b). (c) Result of Hu *et al.*'s method [1]. (d) Result of Sen *et al.*'s method [2]. (e) Result of Kalantari *et al.*'s method [3]. (f) Result of Wu *et al.*'s method [4]. (g) Zoomed-in areas of our result. The proposed UPHDR-GAN handles moving objects better and generates results with fewer ghosting artifacts.

1. Introduction

Dynamic ranges of natural scenes are much wider than those captured by commercial imaging products. Most digital photography sensors often fail to capture the irradiance range that visible to the human eyes. High dynamic range (HDR) imaging techniques have attracted considerable interest because they can overcome such limitations. Some specialized hardware devices [5, 6] have been introduced to produce HDR images directly, but they are usually too expensive to be widely adopted. As a result, computational HDR imaging methods have drawn more attention. The most common strategy is to capture a stack of low dynamic range (LDR) images at different exposure levels and then merge them into an HDR image [7, 8, 9].

Since its first introduction in 1990s, HDR imaging techniques evolve quickly. Some methods [7, 8, 9] are first proposed to reconstruct an HDR image through camera response function (CRF) and then apply tone mapping for display. The original approaches work only for static scenes because they typically assume constant radiance at each pixel over all exposures. If the scenes exist moving content, these methods

produce ghosting artifacts from even small misalignments between exposures. Then, some methods [10, 11, 12] are introduced to fuse inputs with scene motions or dynamic objects using homography or optical flow. Generally, one of the LDR images is considered as the reference image and the other inputs are aligned to the reference. These algorithms can generate high-quality HDR results if inputs are fully aligned, but will suffer from significantly ghosting and blurring artifacts when there are unaligned errors. Some patch-based methods [1, 2] are then proposed to reconstruct the input images by patch-based synthesis according to one selected reference image, to form a fully registered image stack. However, the patch-based reconstruction is not always robust in complicated situations.

Recent works [3, 4, 13] have been proposed to learn the composition process using deep neural networks (DNN). Kalantari *et al.* [3] first proposed a DNN-based HDR generation method, which merges the LDR images after an optical flow-based alignment process. However, their method fails to handle the artifacts and distortions caused by the inevitable optical flow estimation error. Wu *et al.* [4] applied a simple homography to align the background first and used the network to achieve main alignment and fusion. Yan *et al.* [13] introduced an attention-guided network to detect and align dynamic objects before fusion. However, they still suffer from having artifacts when the LDR images contain large motions or significant misalignment, due to the unreliability of image registration. Different techniques are introduced to improve the performance of fusion results, however, the most important problem of deep learning-based methods is that they rely heavily on paired inputs and ground truth.

To relax the constraint of dataset, we propose a GAN-based fusion method to optimize the network using unpaired dataset, named UPHDR-GAN. First, compared to famous single-image enhancement methods [14, 15, 16] and some recent GAN-based image fusion method [17, 18, 19] that are trained on paired dataset, the proposed method trains unpaired dataset and learns mapping from LDR domain to HDR domain. Second, unlike some methods that are designed for unpaired datasets mainly concentrating on processing single-input [20], our UPHDR-GAN is a multi-input method with the consideration of moving objects. Then, even considering multi-input, simply concatenating multi-exposure inputs will suffer from severe ghosting. In contrast, the proposed

method successfully fuses multi-inputs and generates high-quality HDR images without ghosting artifacts by introducing an initialization phase, a modified GAN loss and min-patch training.

Fig. 1 shows the comparisons with several typical de-ghosting methods, including two patch-based methods [1, 2] and two deep learning-based methods [3, 4]. Two patch-based methods use patch matching to align inputs but ignore image integrity. Information lost and undesired halo artifacts appear in final results (Fig. 1(c) and (d)). Kalantari *et al.* [3] applied optical flow to align inputs before they are sent to the network. Flow-based methods often produce deformations caused by the parallax or dynamic contents. Wu *et al.* [4] improved Kalantari’s method and embedded the alignment to the network. Although two DNN-based methods produce satisfactory results in some examples, they still suffer from ghosting artifacts if there are large-scale movements between images (Fig. 1(e) and (f)). Our method deals with the dynamic objects properly with the assistance of the modified GAN loss and min-patch training, which pay more attention to the dynamic regions and emphasize the edges. In addition to visual comparisons, we also organize quantitative comparisons against several typical approaches to validate the superiority of the proposed UPHDR-GAN. In quantitative assessments, the proposed method achieves the best scores on average.

Overall, the main contributions are summarized as follows:

- We proposed a GAN-based multi-exposure HDR fusion network, which relaxes the constraint of paired training dataset and learns the mapping between input and target domains. To our best knowledge, this work is the first GAN-based approach for unpaired HDR reconstruction.
- The proposed method can not only be trained on unpaired dataset but generate HDR results with fewer ghosting artifacts. We apply an initialization phase, a modified GAN loss and min-patch training to avoid ghosting and improve the image quality.
- We provided qualitative and quantitative comparisons with several state-of-the-art methods using UPHDR-GAN, demonstrating its superiority over existing methods.

2. Related Works

2.1. HDR Imaging

HDR imaging has been the subject of extensive research over the past decades, which can be mainly divided into two categories, static and dynamic scene methods.

Static scene methods. Mann *et al.* [7] and Debevec *et al.* [8] first proposed to take sequential LDR images at different exposure levels and then merge them into an HDR image. The original approaches produced spectacular results for static scenes and static cameras. Some variants are then introduced by generating disparity maps or using neural networks. Sun *et al.* computed the disparity map between the stereo images and applied them to compute the CRF [21]. Hashimoto *et al.* developed hard-to-view or nonviewable features and content of color images by a new tone reproduction algorithm [22]. Sheth *et al.* proposed an LDR2HDR network to generate an HDR map of a static scene using differently exposed LDR images [23]. There are also numerous static fusion methods [24, 25, 26, 27, 28, 29] that do not generate HDR outputs but directly obtain informative LDR results. However, due to the lack of an explicit detection for the dynamic objects, the aforementioned methods are unaware of any motion in the scene, so as to be suitable for static scenes only.

Dynamic scene methods. To extend the scope of application, many algorithms introduce the de-ghosting problem from different perspectives, providing solutions that range from rudimentary heuristics to advanced computer vision techniques [30]. The motion-based methods include global exposure registration [31, 32, 33], moving objects removal [34], moving objects selection [35] and moving objects registration [2, 1]. A number of methods reject the moving pixels using weightings in the merging process [36, 37]. Another approach is to detect and resolve ghosting after the merging [38, 39]. Since such methods simply ignore the misaligned pixels, they fail to fully utilize available contents to generate HDR images. Besides, there are also more complicated methods that rely on image registration, which reconstruct each HDR region by searching for the best matching region in LDR images. This is achieved by

pixel (optical flow methods) or patch (patch-based methods) based dense correspondences. For example, Bogoni *et al.* introduced a two-phase alignment strategy, which first performs a global affine registration and then estimates optical flow between input and reference [40]. Zimmer *et al.* presented an energy-based method for estimating the optical flow, which is robust in the presence of noise and occlusion [10]. Also, Sen *et al.* proposed a patch-based energy minimization approach that integrates alignment and HDR reconstruction in a joint optimization [2]. Hu *et al.* handled with saturated regions and moving objects simultaneously, which optimized image alignment based on brightness and gradient consistencies [1]. Although Optical flow based methods are able to align images with complex motions, they usually suffer from deformations in the regions with no correspondences, due to occlusions caused by parallax or dynamic contents. On the other hand, patch-based methods sometimes produce excellent results, while they commonly suffer from low efficiency and usually fail in the presence of large motions and saturated regions. To overcome the issues as above, some deep learning approaches [3, 4, 13] have been developed recently. The deep learning methods have the advantage of exploiting information extracted from training data to identify and compensate for image regions that do not meet the assumptions underlying the HDR process. However, each of these methods only addresses part of the issues and needs paired data to optimize the network. We propose UPHDR-GAN to comprehensively handle existing issues, including solving ghosting artifacts and relaxing the constrain of paired data.

2.2. GAN-based Fusion

The concept of GAN was originally proposed by Goodfellow *et al.* [41], which has drawn substantial attention in the field of deep learning. The vanilla GAN consists of two components, a generator G and a discriminator D , where G is responsible for capturing the data distribution while D tries to distinguish whether a sample comes from the real training data or the generator. This framework corresponds to a min-max two-player game, which provides a powerful way to estimate target distribution and generate new samples. GANs have achieved impressive results in face operation [42, 43, 44], image blending [45], image generation [46, 47], image editing [48],

representation learning [46, 49] and style transfer [50, 20, 51, 52]. Generally, the inputs of the aforementioned methods are noise or a single image. Some recent works are proposed for fusing multi-input images [53, 54, 55, 56, 57]. Perera *et al.* extended unsupervised image-to-image translation to multiple input settings using GAN and validated their method on several tasks, including multi-spectral images to visible image and synthetic to real image translations [53]. Joo *et al.* applied GAN to generate a fusion image with the identity of input image x and the shape of input image y with the help of min-patch training [57]. Guo *et al.* introduced a GAN-based multi-focus image fusion system, which utilized G to generate desired mask maps [54]. Ma *et al.* used GAN to fuse infrared and visible information, obtaining a fused image with major infrared intensities together with additional visible gradients [55, 56]. Recently, there are some GAN-based methods are proposed to handle multi-exposure images [17, 18, 19], Xu *et al.* [17] and Yang *et al.* [18] fused two inputs, the under-exposed image and the over-exposed image, to generate an informative output. Niu *et al.* [19] proposed a reference-based residual merging block for aligning large object motions in the feature domain, and a deep HDR supervision scheme for eliminating artifacts of the reconstructed HDR images. However, these GAN-based methods heavily rely on paired training dataset so that their performances are greatly limited. In comparison, we propose UPHDR-GAN to fuse multi-exposure inputs, which is compatible to unpaired dataset, so that the flexibility and robustness of our proposed network are significantly improved.

3. Method

We propose a GAN-based framework, which is the first method designed for handling unpaired multi-exposure fusion datasets. Like common GAN framework, the generator G learns the mapping function between different domains, while the discriminator D aims to optimize G by distinguishing source domain images from the generated ones. Our collected dataset consists of scenes with and without ground truth. To obtain the unpaired dataset, we upset the organization of input dataset and target dataset. To better describe the framework, we adopt X as source domain data, includ-

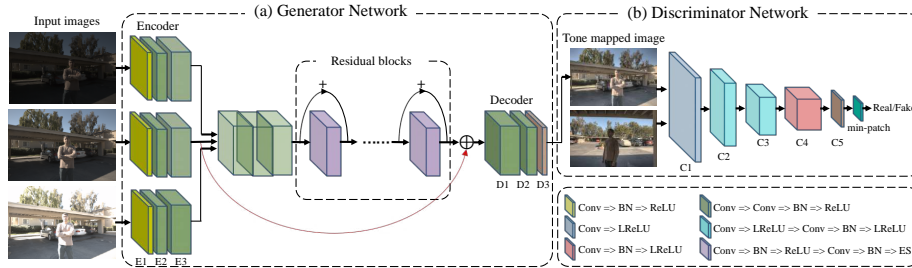


Figure 2: The proposed method seeks to generate high-quality HDR results with unpaired dataset. The architecture of UPHDR-GAN consists of two components operating different functions. **The generator** processes the inputs through down-convolution layers, residual blocks and up-convolution layers so as to generate results with less ghosting. **The discriminator** distinguishes the generated and real HDR images.

ing a wide diversity of multi-exposure sequences $x = \{x_1, x_2, x_3\}$, and a collection of HDR images $\{y_j\}_{j=1, \dots, M} \in Y$, as the target domain data. The data distributions of the two domains are denoted as $x \sim p_{\text{data}}(x)$ and $y \sim p_{\text{data}}(y)$, respectively.

The proposed UPHDR-GAN is capable of generating HDR images with fewer ghosting artifacts in the absence of paired datasets. Its network architecture is introduced in Section 3.1, and the objective function is presented in Section 3.2 in detail.

3.1. Network Architecture

UPHDR-GAN is an images-to-image task with three inputs and one output. The structure of UPHDR-GAN is illustrated in Fig. 2. The generator and the discriminator are simultaneously optimized during the training process. Their detailed layer configurations are presented in Table 1. Instead of feeding the original full-size images into our model, we break down the training images into overlapping patches of size 256×256 patches with a stride of 64. The encoder contains three branches and the input size of each branch is $256^2 \times 6$, which is the concatenation of the inputs $x = \{x_1, x_2, x_3\}$ and their mapped HDR images $H_m = \{H_1, H_2, H_3\}$. H_m is obtained using simple gamma encoding:

$$H_i = \frac{x_i^\gamma}{t_i}, \quad \gamma > 1 \quad (1)$$

where t_i is the exposure time of x_i . The LDRs can facilitate the detection of misalignments and saturation, while the exposure-adjusted HDRs improve the robustness of the

Table 1: Detailed parameter settings of the network, in which ‘BN’ indicates the batch normalization and ‘ES’ represents elementwise sum.

Inputs: $3 \times [256, 256, 6]$							
	Module		Conv			BN	Activation
			Kernel	Stride	Channel	Channel	
<i>Generator</i>	Encoder	E1	7	1	64	64	ReLU
		E2	3	2	128	-	-
			3	1	128	128	ReLU
	E3	3	2	256	-	-	
		3	1	256	256	ReLU	
	Residual blocks		3	2	256	256	ReLU
			3	1	256	256	ES
	Decoder	D1	3	1/2	128	-	-
			3	1	128	128	ReLU
		D2	3	1/2	64	-	-
3	1		64	64	ReLU		
	D3	7	1	3	-	-	
<i>Discriminator</i>		C1	3	1	32	-	LReLU
		C2	3	2	64	-	LReLU
			3	1	64	64	LReLU
		C3	3	2	128	-	LReLU
			3	1	128	128	LReLU
C4	3	1	256	256	LReLU		
	C5	3	1	1	-	-	
Output HDR H_o : [256, 256, 3]							
Tonemapped HDR $T(H_o)$: [256, 256, 3]							

network across LDRs with various exposure levels.

After getting the HDR output H_o , we add a μ -law [3] post-processing to compress the range of image since computing the loss functions on the tone-mapped HDR images is more effective than directly computed in the HDR domain.

$$T(H_o) = \frac{\log(1 + \mu H_o)}{\log(1 + \mu)} \quad (2)$$

where H_o is the output HDR image, μ is a parameter defining the amount of compression and is set to 5,000 in our implementation.

3.1.1. Generator

The generator network is composed of 3 parts, the encoder, eight residual blocks and the decoder. Specifically, the encoder consists of three convolutional blocks: E1,

E2 and E3, as described in Table. 1. Useful local signals are extracted by the encoder for downstream transformation. Afterward, eight residual blocks with identical layout are used to construct the content and the manifold feature. The decoder consists of two identical transposed convolutional blocks (D1 and D2), and a final convolutional layer (D3).

3.1.2. Discriminator

The discriminator network is complementary to the generator. We leverage the technique from PatchGANs [14, 58] to classify each image patch into a real or fake one rather than a full-image discriminator. 70×70 overlapped patches are cropped from generated or real HDR images for training. Such a simple patch-level discriminator uses fewer parameters and can work on images of arbitrary sizes. However, not all regions in the patch contribute to the discriminator optimization during training. If a small part of the generated image is so strange as to be different from the real image, it can be considered as undesirable ghosting artifacts. Therefore, paying more attention to the strangest parts is essential. we applied min-patch training to add a minimum pooling layer at the last part of the PatchGAN (Fig. 3). Note that, minimum pooling is applied to the final output of discriminator if the generator is trained. We acquire the feature maps before min-pooling layer (F) and after min-pooling layer (F_{pool}), respectively. The generator is optimized with F_{pool} , which helps the network focus on the most important parts of the generated images, such as the error parts or strange parts. The discriminator distinguishes the real image from fake image using common PatchGAN and is optimized with features before min-pooling layer F . Min-patch training focuses on the most important part of fake images and helps to avoid ghosting artifacts. In our implementation, the PatchGAN discriminator outputs 64×64 size of feature maps. The min-patch training uses 16×16 min-pooling, so the generator uses output 4×4 size of feature map for training.

3.2. Loss Function

As GAN is a min-max optimization system, the proposed method aims to solve:

$$G^*, D^* = \arg \min_G \max_D L(G, D) \quad (3)$$

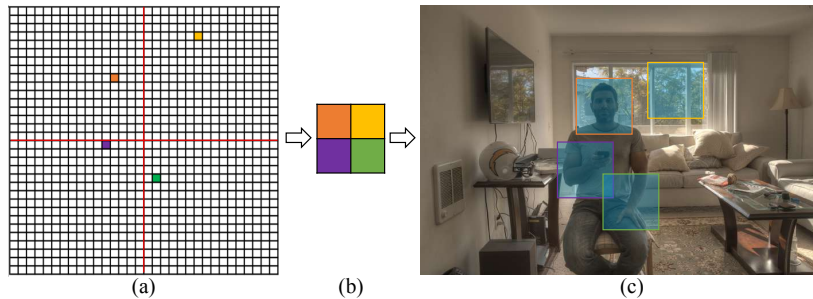


Figure 3: (a) The last feature map of PatchGAN. (b) Minimum pooling is applied to (a). (c) Corresponding respective fields of the input image.

Based on HDR imaging properties, we design our objective function to include the following two losses: (1) the adversarial loss $L_{GAN}(G, D)$, which drives the generator network to achieve the desired manifold transformation; (2) the content loss $L_{con}(G, D)$, which preserves the image content during transformation. The full objective function is:

$$L(G, D) = L_{GAN}(G, D) + w_{con}L_{con}(G, D) \quad (4)$$

where w_{con} is a hyper-parameter to control the relative importance of content loss, so as to balance the effects of transformation and content preservation.

3.2.1. Adversarial Loss

As in classic GAN networks, the adversarial loss is used to constrain the results of G to look like target domain images. In our task, adversarial loss pushes G to generate outputs that are similar to real HDR images in the absence of corresponding ground truth. Meanwhile, D aims to distinguish whether a given image belongs to the synthesized or the real target manifold. However, simply applying the common adversarial loss is not sufficient for preserving clear edge information. For this reason, Chen *et al.* [51] proposed to confuse D with a blur dataset to push generator to produce images with sharp edges, which has been proven useful for style transformation. Similarly, we also add a blur HDR dataset to facilitate G to generate clearer output. Specifically, from the target images $\{y_j\}_{j=1,\dots,M} \in Y$, we generate the same number of blur images $\{c_j\}_{j=1,\dots,M} \in C$ by removing clear edges in Y . In details, for each y_j , we apply

the following three steps:

1. Detecting edge pixels using a standard Canny edge detector;
2. Dilating the edge regions;
3. Applying a Gaussian smoothing in the dilated edge regions.

In other words, the discriminator tries to correctly classify an image into three categories: the generated image $G(x)$, the real HDR image y , and the blurred HDR image c , as formulated in Eq. 5.

$$\begin{aligned}
 L_{\text{GAN}} = & \mathbb{E}_{y \sim p_{\text{data}}(y)} [\log D(y)] \\
 & + \mathbb{E}_{c \sim p_{\text{data}}(c)} [\log(1 - D(c))] \\
 & + \mathbb{E}_{x \sim p_{\text{data}}(x)} [\log(1 - D(G(x)))]
 \end{aligned} \tag{5}$$

3.2.2. Content Loss

The adversarial loss just ensures that the generated image looks realistic in the target domain, therefore it is inadequate to result in a transformation that preserves semantic information of the input alone. It is essential to enforce a more strict constraint to ensure semantic consistency between the inputs and the output. Generally, the middle-exposure image is selected as the reference and other inputs are aligned to the reference. We define the image content loss that computes the difference between the middle-exposure input and the generated HDR result. Instead of using common L_2 loss function, we apply perceptual loss [50] to measure high-level semantic differences. As such, the complete image content loss is defined as:

$$L_{\text{con}}(G, D) = \mathbb{E}_{x \sim p_{\text{data}}(x)} [\|VGG_l(G(x)) - VGG_l(x)\|_1] \tag{6}$$

where l refers to a specific layer in the VGG network, and we apply the ‘conv4_4’ layer in our implementation.

The hyper-parameter w_{con} is added to balance the adversarial loss and content loss. A larger w_{con} produces images with more content information from the middle-exposure input, generating images that do not like desired HDR images. However, a small w_{con} learn the translation excessively so that the semantic content information cannot be well preserved. To strike a balance, we set w_{con} to be 1.5 at the initial stage

Table 2: Detailed source information of our dataset.

Source Name	URL	Number
HDReye	https://mmspg.epfl.ch/downloads/hdr-eye/	46
Fairchild	http://rit-mcsl.org/fairchild/HDRPS/HDRthumbs.html	103
EmpaMT	http://empamedia.ethz.ch/hdrdatabase/index.php	30
Kalantari [3]	https://cseweb.ucsd.edu/~viscomp/projects/SIG17HDR	70
Tursun [59]	http://user.ceng.metu.edu.tr/~akyuz/files/eg2016/index.html	17

to correctly preserve content information with moderate transformation. Then, w_{con} is gradually decreased to obtain better transformation results as training becomes increasingly stable and the semantic content information has been properly reconstructed at the initial stage. The variation trend of w_{con} is described as:

$$w_{con} = w_{con} \times 0.96^{\lfloor N_e/10 \rfloor} \quad (7)$$

where N_e is the number of epochs in the training process.

4. Experiments

We first illustrate the datasets and implementation details in Section 4.1 and then conduct comprehensive experiments to verify the performance of the proposed method, including quantitative comparisons (Section 4.2), qualitative comparisons (Section 4.3) and ablation studies (Section 4.4). Specifically, we first compare our method with several methods that are just suitable for static inputs [25, 27, 26, 28, 29, 17], and then compare with several classic de-ghosting methods, including two patch-based methods [2, 1], and two deep neural network (DNN) mergers with and without optical flow registration, respectively [3, 4]. In order to make a fair comparison, we collect the codes from the authors of the above algorithms to generate their results with default settings. Xu *et al.* combined two inputs, the under-exposed image and over-exposed image, to generate an output [17]. We remove the mid-exposure images from the test set when we evaluate their method.

4.1. Datasets and Implementation Details

Training deep networks usually require a large number of training examples, which potentially determines the upper bound of a network. The datasets of common deep



Figure 4: Results of the initialization phase. (a) A middle-exposure input. (b) Generated result after 10 epochs pre-training.

learning-based fusion methods usually include a set of LDR images of a dynamic scene and their corresponding HDR image. However, most existing HDR datasets either lack ground truth images [30, 59], or have a small number of scenes with only rigid motion [60]. Although Kalantari *et al.* introduced the first HDR dataset, the variety of the scenes is so limited [3]. UPHDR-GAN relaxes the constraints of paired input, which learns the mapping between input and target domains and transforms the multi-inputs to an informative HDR output. We have collected a total of 266 groups of images from various sources, including static/dynamic, indoor/outdoor and daytime/nighttime scenes, as seen in Table 2 for the detailed information. By disorganizing their correspondence between the inputs and ground truth, the unpaired dataset is obtained. Some of them include approximately 10 multi-exposure inputs, from which we select 3 images with minimum, medium and maximum exposure as training inputs. For the training data, we first align them using a simple homography transformation, making the learning more effective than directly training it without background alignment. Then, we break down the training images into overlapping patches of size 256×256 patches with a stride of 64, and then perform data augmentation (flipping and rotation), further increasing the training data by 8 times.

We implement UPHDR-GAN in PyTorch and all the experiments are performed on an NVIDIA RTX 2080Ti GPU. Adam optimizer is applied with the learning rate of 2.0×10^{-4} for the generator and the discriminator. An initialization phase is introduced to improve the convergence and avoid training being trapped in a suboptimal local minimum. We initialize the generator that reconstructs the content of middle-exposure

Table 3: Quantitative comparison of proposed method with several classic static methods based on twenty static scenes. **Red** color indicates the best performance and **blue** color indicates the second best results.

	PSNR	SSIM	HDR-VDP-2
Mertens [25]	29.817	0.9511	54.056
Li2012 [26]	30.289	0.9527	53.925
Li2013 [27]	31.020	0.9575	55.142
Paul [28]	31.876	0.9584	55.953
Ma [29]	33.469	0.9675	57.329
Xu [17]	32.582	0.9651	53.631
Ours	40.513	0.9715	60.019

Table 4: Quantitative comparison of proposed method with several state-of-the-art de-ghosting methods based on twenty dynamic scenes. **Red** color indicates the best performance and **blue** color indicates the second best results.

	PSNR	SSIM	HDR-VDP-2
Sen [2]	40.924	0.9806	56.239
Hu [1]	34.785	0.9725	55.754
Kalantari [3]	42.532	0.9871	59.824
Wu [4]	41.667	0.9844	59.908
Ours	42.857	0.9869	60.052

input and ignores the translation. For this purpose, we pre-train the generator G using merely L_{con} . An example is presented in Fig. 4. After 10 epochs pre-training, the network properly reconstructs the content information of middle-exposure input. Since we select it as the reference, the initialization helps to avoid ghosting.

4.2. Quantitative Comparisons

The main goal of image fusion is to integrate complementary information from multiple sources so that the fused images are more suitable for the purpose of human visual perception and computer processing. Although the proposed method can generate high-quality HDR images without ground truth, we select the test set for quantitative comparisons from paired datasets that include multi-exposure inputs and HDR images. As the ground truth is available, we can conduct various quantitative evaluations and comparisons. We first compute the Peak Signal to Noise Ratio (PSNR) [61]

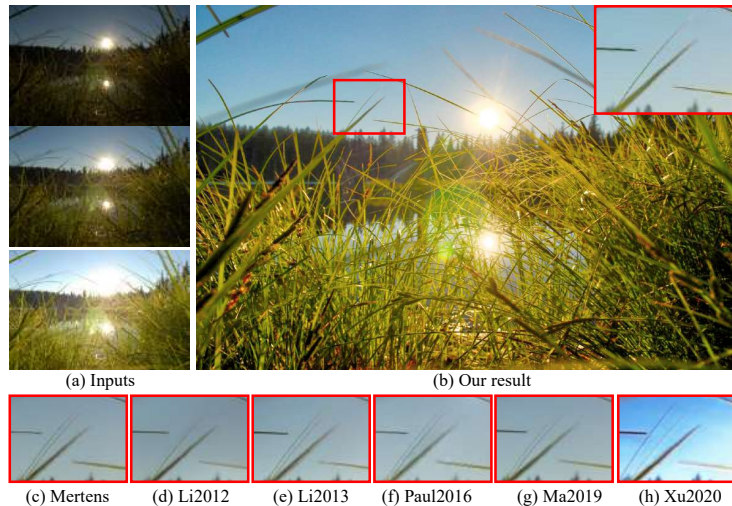


Figure 5: Visual comparisons on the testing data from EmpaMT dataset. (a) Input LDR images. (b) Our result. (c) Result of Mertens *et al.*'s method [25]. (d) Result of Li *et al.*'s method [26]. (e) Result of Li *et al.*'s method [27]. (f) Result of Paul *et al.*'s method [28]. (g) Result of Ma *et al.*'s method [29]. (h) Result of Xu *et al.*'s method [17].

and Structural Similarity Index Measure (SSIM) [62] scores between the generated image and the real image. We also compute the HDR-VDP-2 [63], a metric specifically designed for measuring the visual quality of HDR images. For the two parameters used to compute the HDR-VDP-2 scores, we set the diagonal display size to 24 inches, and the viewing distance to 0.5 meters.

Twenty static scenes and twenty dynamic scenes, which include multi-inputs and corresponding ground truth, are collected as the test set for quantitative comparisons. The static sequences are either captured by cameras mounted on a tripod or aligned before the fusion calculation. Our method is compared with several classic methods that are suitable for static inputs [25, 26, 27, 28, 29, 17] on these static scenes and the comparison results are shown in Table 3. These static methods fuse multi-exposure inputs with the absence of ground truth, and therefore resulting in lower scores when computing the difference between output and ground truth. The proposed UPHDR-GAN also abandons the constraint of ground truth, but can extract information from target HDR dataset, hence providing results with better PSNR, SSIM and HDR-VDP-2 values on



Figure 6: Visual comparisons with de-ghosting methods. (a) Input images. (b) Result of Hu *et al.*'s method [1]. (c) Result of Sen *et al.*'s method [2]. (d) Result of Kalantari *et al.*'s method [3]. (e) Result of Wu *et al.*'s method [4]. (f) Our result. We compare the zoomed-in local areas of UPHDR-GAN and other de-ghosting methods. Our method owns the best performance overall.

average. Table 4 exhibits the comparison results of UPHDR-GAN with several de-ghosting methods. Two patch-based methods [2, 1] reconstruct the underlying image stacks by patch match oriented optimization. Kalantari *et al.* [3] and Wu *et al.* [4] obtain HDR results through deep neural networks. Although these methods in Table 4 get similar quantitative scores, the proposed method owns superior performance overall.

4.3. Qualitative Comparisons

In this section, our method is first compared with [25, 27, 26, 28, 29, 17] on a static scene (Fig. 5). The compared methods are mature enough to handle images that are static, but ignore the tiny motions, such as the moving leaves caused by wind. Some slight movements of the left leaves in Fig. 5 lead to ghosting artifacts of the compared methods. Although some of them have strategies to tackle with dynamic contents, such as median and recursive filters of [26], they still produce unsatisfactory ghosting. Xu *et al.* solely obtained information from the under-exposed image and over-exposed image [17], which leads to the mediocre result with color deviation.

Fig. 6 and Fig. 7 show the qualitative comparisons against several state-of-the-art de-ghosting methods [1, 2, 3, 4]. Two patch-based approaches [1, 2] aim to recon-

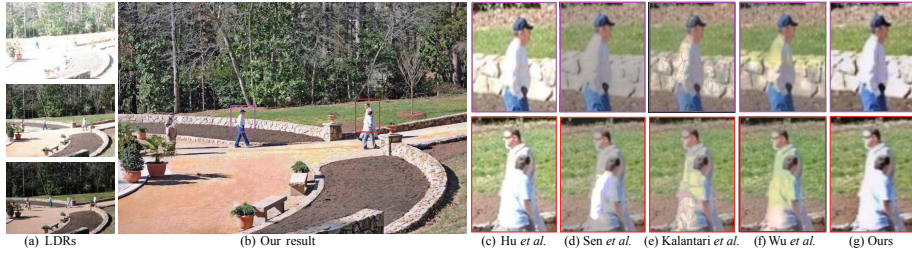


Figure 7: Visual comparisons with de-ghosting methods. (a) Input images. (b) Our result. (c) Result of Hu *et al.*'s method [1]. (d) Result of Sen *et al.*'s method [2]. (e) Result of Kalantari *et al.*'s method [3]. (f) Result of Wu *et al.*'s method [4]. (g) Zoomed-in areas of our result. The scene is challenging because there are large foreground motions between input LDR images. The proposed UPHDR-GAN can properly deal with the motions caused by moving people.

struct ghost regions in the output image by transferring information from inputs which are determined by patch matching. However, they can not recover the structured regions properly. The errors in motion estimation are difficult to avoid in the presence of tiny random motions for patch-based methods although they generally produce relatively good results. Hu's method generates results with undesirable artifacts around the building (red arrow in Fig. 6(b)) and Sen's method gets results with serious halo artifacts (yellow arrows in Fig. 6). Note that, Hu's method tends to suffer from color drifting in some cases, which occurs in computing generic intensity mapping function and then causes the radiance consistency measure to be ineffective.

Deep learning methods have the advantage that they can exploit information extracted from training data to identify and compensate for image regions. However, they only perform well in one way or another. Kalantari *et al.* [3] applied optical flow to align inputs first and then sent them to a conventional neural network to obtain fused results, which may produce artifacts due to two main reasons: misalignment of optical flow and the limitation of merging process. Wu *et al.* [4] improved Kalantari *et al.*'s method and embedded the alignment into the network. The two methods adopt similar network architecture and produce unnatural transformations in the sky region in Fig. 6 (green arrows) and ghosting artifacts in Fig. 7. Our method can properly handle such problems and obtain results with higher sensory experience.

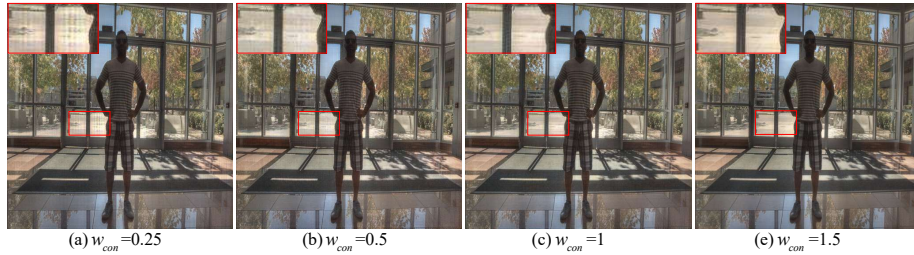


Figure 8: The effect of different w_{con} . We set w_{con} to be 1.5 at the initial stage to keep a balance between transformation and content preservation.

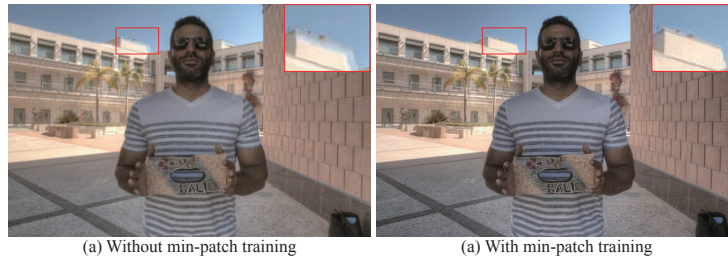


Figure 9: The influence of min-patch training. (a) The generated result without min-patch training. (b) The generated result with min-patch training.

4.4. Ablation Studies

We perform the ablation studies of different items to understand how these main modules contribute to final results, which show that each component plays an important role in our architecture.

4.4.1. Ablation Study of w_{con}

We first conduct some experiments to illustrate why we set $w_{con} = 1.5$ at the initial stage. Fig. 8 shows corresponding results when we select different w_{con} . Smaller w_{con} cannot generate desired details or suffer from ghosting artifacts because they tend to learn the translation but ignore to preserve the semantic content information. We set w_{con} to be 1.5 at the initial stage to keep a balance between transformation and content preservation. It correctly maintains semantic content with enjoyable transformation (Fig. 8(a)-(c)). If we continue to increase the value of w_{con} , the results will be similar to middle-exposure LDR image because they bring more content information from the

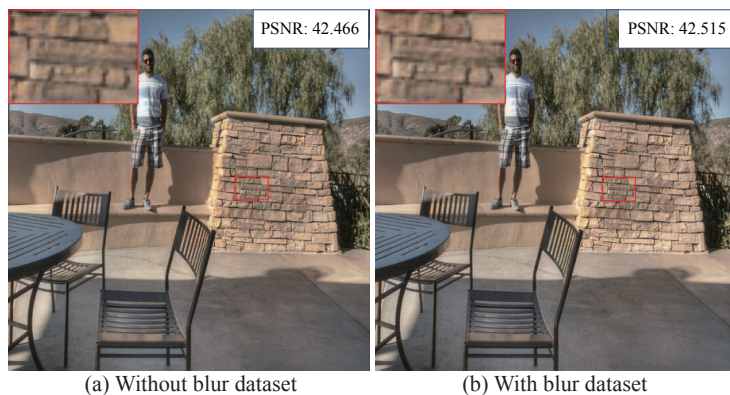


Figure 10: The influence of blur dataset. (a) Result without blur dataset. (b) Result with blur dataset.

input photo so that the details of yard and floor regions cannot be generated.

4.4.2. Ablation Study of Min-patch Training

Common discriminator can distinguish the generated images and real images. However, not all regions contribute to the discriminator optimization during training. If a small part of the generated image is so strange as to be different from real image, it can be considered as undesirable ghosting artifacts. We add min-patch training to detect such regions and avoid ghosting artifacts. Fig. 9 shows the effectiveness of min-patch training. After the min-patch training, UPHDR-GAN gets result with fewer artifacts (Fig. 9(b)) compared to result without min-patch training (Fig. 9(a)).

4.4.3. Ablation Study of Blur Dataset

Simply applying GAN loss is not sufficient for generating sharp HDR images. This is because clear edges is an important characteristic of HDR images, but common GAN loss may produce results with unclear edges. To solve the problem, we add a blur dataset C as fake images to confuse the discriminator to produce images with sharp edges. Fig. 10 shows the influence of the blur dataset, in which the result with blur dataset (Fig. 10(b)) has more sharp edges and higher PSNR values.

5. Conclusion

We have presented a novel method for fusing multi-exposure images with unpaired datasets. The proposed method relaxes the constraints that deep learning-based methods need paired inputs and ground truth by introducing generative adversarial networks. The proposed method learns the translation between input domain and target domain and transforms the multi-inputs into an informative HDR output. It offers the prospect for more extensive applications of HDR imaging. However, generative adversarial networks obtain unclear results sometimes. We applied some techniques to generate images with sharp edges and clear content information, and we will further focus on the aspect to explore more useful algorithms. We conduct comprehensive comparisons, include quantitative assessment and qualitative comparisons, with several typical methods to demonstrate the effectiveness of UPHDR-GAN.

References

- [1] J. Hu, O. Gallo, K. Pulli, X. Sun, Hdr deghosting: How to deal with saturation?, in: Proc. CVPR, 2013, pp. 1163–1170.
- [2] P. Sen, N. K. Kalantari, M. Yaesoubi, S. Darabi, D. B. Goldman, E. Shechtman, Robust patch-based hdr reconstruction of dynamic scenes., ACM Trans. Graph 31 (6) (2012) 1–11.
- [3] N. K. Kalantari, R. Ramamoorthi, Deep high dynamic range imaging of dynamic scenes, ACM Trans. Graph 36 (4) (2017) 144.
- [4] S. Wu, J. Xu, Y. Tai, C. Tang, Deep high dynamic range imaging with large foreground motions, in: Proc. ECCV, 2018, pp. 120–135.
- [5] S. K. Nayar, T. Mitsunaga, High dynamic range imaging: Spatially varying pixel exposures, in: Proc. CVPR, 2000, pp. 472–479.
- [6] J. Tumblin, A. Agrawal, R. Raskar, Why i want a gradient camera, in: Proc. CVPR, 2005, pp. 103–110.

- [7] S. Mann, R. W. Picard, On being 'undigital' with digital cameras: Extending dynamic range by combining differently exposed pictures, in: *Proceedings of IS and T*, 1995, pp. 442–448.
- [8] P. Debevec, J. Malik, Recovering high dynamic range radiance maps from photographs, in: *Conference on Computer Graphics & Interactive Techniques*, 1997, pp. 369–378.
- [9] E. Reinhard, G. Ward, S. Pattanaik, P. Debevec, *High dynamic range imaging : acquisition, display, and image-based lighting*, Princeton University Press, 2010.
- [10] H. Zimmer, A. Bruhn, J. Weickert, Freehand hdr imaging of moving scenes with simultaneous resolution enhancement, *Computer Graphics Forum* 30 (2) (2011) 405–414.
- [11] Z. L. Szpak, W. Chojnacki, A. Eriksson, A. V. Den Hengel, Sampson distance based joint estimation of multiple homographies with uncalibrated cameras, *Computer Vision and Image Understanding* 125 (2014) 200–213.
- [12] T. Oh, J. Lee, Y. Tai, I. S. Kweon, Robust high dynamic range imaging by rank minimization, *IEEE Trans. on Pattern Analysis and Machine Intelligence* 37 (6) (2015) 1219–1232.
- [13] Q. Yan, D. Gong, Q. Shi, A. V. Den Hengel, C. Shen, I. Reid, Y. Zhang, Attention-guided network for ghost-free high dynamic range imaging, in: *Proc. CVPR*, 2019, pp. 1751–1760.
- [14] P. Isola, J.-Y. Zhu, T. Zhou, A. A. Efros, Image-to-image translation with conditional adversarial networks, in: *Proc. CVPR*, 2017, pp. 1125–1134.
- [15] M. Gharbi, J. Chen, J. T. Barron, S. W. Hasinoff, F. Durand, Deep bilateral learning for real-time image enhancement, *ACM Trans. Graph* 36 (4) (2017) 118.
- [16] C. Li, J. Guo, F. Porikli, Y. Pang, Lightnet: A convolutional neural network for weakly illuminated image enhancement, *Pattern Recognition Letters* 104 (2018) 15–22.

- [17] H. Xu, J. Ma, X.-P. Zhang, Mef-gan: multi-exposure image fusion via generative adversarial networks, *IEEE Trans. on Image Processing* 29 (2020) 7203–7216.
- [18] Z. Yang, Y. Chen, Z. Le, Y. Ma, Ganfuse: a novel multi-exposure image fusion method based on generative adversarial networks, *Neural Computing and Applications* (2020) 1–13.
- [19] Y. Niu, J. Wu, W. Liu, W. Guo, R. W. Lau, Hdr-gan: Hdr image reconstruction from multi-exposed ldr images with large motions, *arXiv preprint arXiv:2007.01628*.
- [20] J.-Y. Zhu, T. Park, P. Isola, A. A. Efros, Unpaired image-to-image translation using cycle-consistent adversarial networks, in: *Proc. ICCV, 2017*, pp. 2223–2232.
- [21] N. Sun, H. Mansour, R. K. Ward, Hdr image construction from multi-exposed stereo ldr images, in: *Proc. ICIP, 2010*, pp. 2973–2976.
- [22] A. R. Varkonyi-Cozy, A. Rovid, T. Hashimoto, Gradient-based synthesized multiple exposure time color hdr image, *IEEE Trans. on Instrumentation and Measurement* 57 (8) (2008) 1779–1785.
- [23] K. Sheth, Deep neural networks for hdr imaging, *arXiv preprint arXiv:1610.07629*.
- [24] P. J. Burt, The pyramid as a structure for efficient computation, in: *Multiresolution image processing and analysis, 1984*, pp. 6–35.
- [25] T. Mertens, J. Kautz, F. Van Reeth, Exposure fusion, *Computer Graphics Forum* 28 (1) (2007) 382–390.
- [26] S. Li, X. Kang, Fast multi-exposure image fusion with median filter and recursive filter, *IEEE Trans. on Consumer Electronics* 58 (2) (2012) 626–632.
- [27] S. Li, X. Kang, J. Hu, Image fusion with guided filtering, *IEEE Trans. on Image Processing* 22 (7) (2013) 2864–2875.

- [28] S. Paul, I. S. Sevcenco, P. Agathoklis, Multi-exposure and multi-focus image fusion in gradient domain, *Journal of Circuits, Systems and Computers* 25 (10) (2016) 1650123.
- [29] K. Ma, Z. Duanmu, H. Zhu, Y. Fang, Z. Wang, Deep guided learning for fast multi-exposure image fusion, *IEEE Trans. on Image Processing* 29 (2019) 2808–2819.
- [30] O. T. Tursun, A. Erdem, E. Erdem, The state of the art in hdr deghosting: A survey and evaluation, *Computer Graphics Forum* 34 (2) (2015) 683–707.
- [31] A. Tomaszewska, R. Mantiuk, Image registration for multiexposure high dynamic range image acquisition, in: *International Conference on Computer Graphics, Visualization and Computer Vision*, 2007.
- [32] S. B. Kang, M. T. Uyttendaele, S. Winder, R. Szeliski, High dynamic range video, *ACM Trans. Graph* 22 (3) (2003) 319–325.
- [33] K. Jacobs, C. Loscos, G. Ward, Automatic high-dynamic range image generation for dynamic scenes, *IEEE Computer Graphics and Applications* 28 (2) (2008) 84–93.
- [34] W. Zhang, W. K. Cham, Gradient-directed composition of multi-exposure images, in: *Proc. CVPR, 2010*, pp. 530–536.
- [35] C. Lee, Y. Li, V. Monga, Ghost-free high dynamic range imaging via rank minimization, *IEEE Signal Processing Letters* 21 (9) (2014) 1045–1049.
- [36] E. A. Khan, A. O. Akyüz, E. Reinhard, Ghost removal in high dynamic range images, in: *Proc. ICIP, 2006*, pp. 2005–2008.
- [37] Y. S. Heo, K. M. Lee, S. U. Lee, Y. Moon, J. Cha, Ghost-free high dynamic range imaging, *Asian Conference on Computer Vision* (2010) 486–500.
- [38] O. Gallo, N. Gelfandz, W. Chen, M. Tico, K. Pulli, Artifact-free high dynamic range imaging, in: *International Conference on Computational Photography*, 2009, pp. 1–7.

- [39] S. Raman, S. Chaudhuri, Reconstruction of high contrast images for dynamic scenes, *The Visual Computer* 27 (12) (2011) 1099–1114.
- [40] L. Bogoni, Extending dynamic range of monochrome and color images through fusion, in: *Proc. ICPR*, 2000, pp. 7–12.
- [41] I. Goodfellow, J. Pougetabadie, M. Mirza, B. Xu, D. Wardefarley, S. Ozair, A. Courville, Y. Bengio, Generative adversarial nets, in: *Proc. NIPS*, 2014, pp. 2672–2680.
- [42] J. Cheng, Y.-P. P. Chen, M. Li, Y. Jiang, Tc-gan: Triangle cycle-consistent gans for face frontalization with facial features preserved, in: *ACM Multimedia*, 2019, pp. 220–228.
- [43] Y. Sun, S. Liu, D. Zhu, R. Bao, W. Wang, X. Shu, S. Yan, Face aging with contextual generative adversarial nets, in: *ACM Multimedia*, 2017, pp. 82–90.
- [44] Q. Yan, T. Li, R. Qian, C. Dong, S. Liu, W. Zhu, L. Lin, Beautygan: Instance-level facial makeup transfer with deep generative adversarial network, in: *ACM Multimedia*, 2018, pp. 645–653.
- [45] H. Wu, S. Zhang, J. Zhang, K. Huang, Gp-gan: Towards realistic high-resolution image blending, in: *ACM Multimedia*, 2019, pp. 2487–2495.
- [46] A. Radford, L. Metz, S. Chintala, Unsupervised representation learning with deep convolutional generative adversarial networks, in: *Proc. ICLR*, 2016.
- [47] Y. Lu, S. Wu, Y. Tai, C. Tang, Image generation from sketch constraint using contextual gan, in: *Proc. ECCV*, 2018, pp. 205–220.
- [48] J. Zhu, P. Krahenbuhl, E. Shechtman, A. A. Efros, Generative visual manipulation on the natural image manifold, in: *Proc. ECCV*, 2016, pp. 597–613.
- [49] T. Salimans, H. Zhang, A. Radford, D. Metaxas, Improving gans using optimal transport, *arXiv preprint arXiv:1803.05573*.

- [50] J. Johnson, A. Alahi, L. Fei-Fei, Perceptual losses for real-time style transfer and super-resolution, in: Proc. ECCV, 2016, pp. 694–711.
- [51] Y. Chen, Y.-K. Lai, Y.-J. Liu, Cartoongan: Generative adversarial networks for photo cartoonization, in: Proc. CVPR, 2018, pp. 9465–9474.
- [52] B. He, F. Gao, D. Ma, B. Shi, L. Duan, Chipgan: A generative adversarial network for chinese ink wash painting style transfer, in: ACM Multimedia, 2018, pp. 1172–1180.
- [53] P. Perera, M. Abavisani, V. M. Patel, In2i: Unsupervised multi-image-to-image translation using generative adversarial networks, in: Proc. ICPR, 2018, pp. 140–146.
- [54] X. Guo, R. Nie, J. Cao, D. Zhou, L. Mei, K. He, Fusegan: Learning to fuse multi-focus image via conditional generative adversarial network, IEEE Trans. on Multimedia 21 (8) (2019) 1982–1996.
- [55] J. Ma, W. Yu, P. Liang, C. Li, J. Jiang, Fusiongan: A generative adversarial network for infrared and visible image fusion, Information Fusion 48 (2019) 11–26.
- [56] J. Ma, H. Xu, J. Jiang, X. Mei, X.-P. Zhang, Ddcgan: A dual-discriminator conditional generative adversarial network for multi-resolution image fusion, IEEE Trans. on Image Processing 29 (2020) 4980–4995.
- [57] D. Joo, D. Kim, J. Kim, Generating a fusion image: One’s identity and another’s shape, in: Proc. CVPR, 2018, pp. 1635–1643.
- [58] C. Li, M. Wand, Precomputed real-time texture synthesis with markovian generative adversarial networks, in: Proc. ECCV, 2016, pp. 702–716.
- [59] O. T. Tursun, A. O. Akyüz, A. Erdem, E. Erdem, An objective deghosting quality metric for hdr images, Computer Graphics Forum 35 (2) (2016) 139–152.
- [60] K. Karadzovichadziabdic, J. H. Telalovic, R. Mantiuk, Subjective and objective evaluation of multi-exposure high dynamic range image deghosting methods, in: Eurographics, 2016, pp. 29–32.

- [61] P. C. Teo, D. J. Heeger, Perceptual image distortion, in: Proc. ICIP, Vol. 2, 1994, pp. 982–986.
- [62] Z. Wang, A. C. Bovik, H. R. Sheikh, E. P. Simoncelli, Image quality assessment: from error visibility to structural similarity, IEEE Trans. on Image Processing 13 (4) (2004) 600–612.
- [63] R. Mantiuk, K. J. Kim, A. G. Rempel, W. Heidrich, Hdr-vdp-2: A calibrated visual metric for visibility and quality predictions in all luminance conditions, ACM Trans. Graph 30 (4) (2011) 1–14.